Journal Name

ARTICLE

Morphological adaptability of graphitic carbon nanofibers to enhance sodium insertion in a diglyme-based electrolyte

Received 00th January 20xx,
Accepted 00th January 20xx

DOI: 10.1039/x0xx00000x

www.rsc.org/

Francisco Nacimiento, Marta Cabello, Gregorio F. Ortiz*, Ricardo Alcántara, Pedro Lavela and José L. Tirado

The recent introduction of glyme-based solvents has opened new opportunities to characterize graphitic materials as anodes for sodium-ion batteries. We evaluate the electrochemical behaviour of a graphitized carbon nanofiber for the first time. X-ray diffraction, electron paramagnetic resonance and nuclear magnetic resonance allow to untangle a sodium insertion mechanism in which the occurrence of an activation process during the first discharge enhances sodium accessibility to active redox centres at the interlayer space. Morphological changes observed by electron microscopy could be responsible for this behaviour. A full graphitized carbon nanofibers/$NaPF_6$(diglyme)/$Na_3V_2(PO_4)_3$ sodium-ion battery will be tested to probe the reliability of this graphitic nanostructure as negative electrode.

Introduction

Sodium-ion batteries are regarded as an actual alternative to lithium-ion batteries, mainly because of the highly abundant mineral resources, low cost and safety issues. Consequently, the efforts for searching sodium-intercalating materials are rapidly growing in the last years. The vast knowledge acquired on insertion materials for Li-ion batteries have speed up the development of positive electrodes performing good capacity and cyclability such as layered oxides and NASICON based phosphates, among others.[1-3] Concerning anodes, a wide variety of low potential materials have been found to react with sodium through similar mechanism than lithium. Thus, carbonaceous materials, alloying metals, titanium-based compounds and oxides driving conversion reactions have revealed low potential electrochemical reactions with potential applicability as negative electrodes.[4-6] Nevertheless, issues affecting to the reversibility of the sodium reaction remain still unresolved, similarly to their lithium analogues. The high abundance of carbonaceous materials allows to prepare electrodes at low cost and hence they attract much attention since the beginning of research on Na batteries. Particularly, the initial search for a suitable graphitic material was hindered by the irreversible intercalation of sodium into graphite using the most common carbonate-based electrolytes.[7] An alternative approach was the use of non-graphitizable carbons. The unique porous structure provided by hard carbons have revealed to be an optimal allocation for Na^+ ions which render a low potential plateau.[8-10] However, it is well-known that the electrolyte composition could play an important role to optimize the electrochemical performance.[11] Na-ion insertion in graphite is poor in the absence of solvent cointercalation. Thus, by using quantum-mechanical calculations ascribed this phenomenon to the competition between the ionization of the metal atom, and the ion–substrate coupling.[12] Using DFT calculations showed the lack of covalent component that helps stabilize the intercalated layered material, as compared with Lithium.[13] On the contrary, the reduced repulsion in the larger solvated sodium ion resulted in higher stability in the discharged graphite.[14-16] Hopefully, the use of glyme-based solvents has opened new opportunities for graphitized materials, because they stabilized the graphitic structure by allowing the cointercalation of sodium-solvent assemblies and staging mechanism.[14,17-20] Surprisingly, although the cointercalation of solvent together with lithium into graphite is harmful for the battery, it is an advantage in the case of sodium. This breakthrough has allowed to revise the electrochemical insertion of sodium in graphitic materials.

An alternative strategy to promote the use of carbonaceous materials is the search for nanosized materials. Morphology control and size diminution are effective strategies to ameliorate mass transport and storage, hence improving the electrochemical performance.[24] Nanostructured materials such as hollow carbons,[25] nanobubbles,[26] nanosheets,[27] have been reported recently as anodes. Particularly, carbon nanofibers (CNF) have attracted much attention.[28,29] The special morphology and small diameter of the fibers are very suitable for a fast battery charge/discharge. To our knowledge, all these examples correspond to materials pyrolyzed at temperatures lower than 1000ºC. In this work, we study the intercalation of sodium into a graphitized nanofiber for the first time. The limited reversibility of the sodium intercalation in its ordered

[a] Departamento de Química Inorgánica e Ingeniería Química, Instituto Universitario de Investigación en Química Fina y Nanoquímica IUNAN, Universidad de Córdoba, Campus de Rabanales, Edificio Marie Curie, E-14071 Córdoba, Spain. E-mail: g72maorg@uco.es

† Footnotes relating to the title and/or authors should appear here.
Electronic Supplementary Information (ESI) available: [details of any supplementary information available should be included here]. See DOI: 10.1039/x0xx00000x

structure I overcome by using a diglyme-based electrolyte. The insertion mechanism will be unveiled by performing X-ray diffraction, resonance paramagnetic and ^{23}Na NMR spectroscopies. In addition, a full CNF / $Na_3V_2(PO_4)_3$ sodium-ion battery will be eventually tested. The morphology of carbon nanofibers (CNF) with structural and surface defects due to the mixed features of disordered and graphitic carbon, played an important role in the improvement of the lithium ion storage and the rate-determining reactions during the topotactic process.[30] Therefore, we think we can transfer this knowledge to Na-ion batteries when combining with diglyme-based electrolytes.

Experimental

A PR24 carbon nanofiber, supplied by Pyrograf Products Inc., was employed. These nanofibers were previously purified and activated by treating with nitric acid solution, then washed with deionized water and finally dried under vacuum at 120°C. A C@$Na_3V_2(PO_4)_3$ sample (NVP), with a NASICON-type structure, was prepared a ball milling assisted solid state reaction as described in elsewhere.[31]

In order to study the crystallographic structure, X-ray diffraction (XRD) patterns were recorded using a Bruker D8 Discover A25 equipment provided with Cu Kα radiation, Ge monochromator, Lynxeye detector and 0.04°2θ steps. In order to record the XRD patterns of the electrodes retrieved from the electrochemical cells, Kapton-tape was used to provide a protective atmosphere. The lattice parameters were determined by using TOPAS software. The particle morphology was examined by Field-Emission Scanning Electron Microscopy (FESEM) in a A JSM-7800F Prime microscope furnished with a EDX analyzer. Also, Scanning Electron Microscopy (TEM) images were recorded in a JEOL 1400 microscope.

Room temperature EPR spectra of samples introduced in EPR quartz tubes were recorded in a EMX micro X-band instrument from Bruker, with a resonance frequency of 9.75 GHz. The sample was previously outgassed by heating under vacuum. ^{23}Na MAS NMR spectra of the electrodes were recorded in a Bruker instrument at 12 kHz of spin rate, with pulse 15º, 60000 accumulations and delay time 0.1 s. Samples retrieved from cycled sodium half cells were disassembled and the electrode material was transferred to a hermetically sealed sample holder into a glove box.

Sodium half-cells were assembled in two-electrode Swagelok™-type cells mounted in an Ar-filled glove box. For this purpose, the working electrode was prepared by homogeneously mixing CNF (92%) and PVDF (polyvinylidene fluoride) (8%) in N-methyl-2-pyrrolidone and spreading the resulting paste onto a copper disk with 9 mm of diameter. The counter electrode was a 9 mm sodium disk. Both electrodes were separated by glass fiber disks (GF/A-Whatman) impregnated with a 1M $NaPF_6$ in diglyme (DGM) electrolyte solution. Galvanostatic experiments were performed at different C/n rates, being n the number of hours needed for the insertion of one sodium per formula unit at the applied current intensity. Cyclic voltammetry (CV) was performed in three-electrode Swagelok™-type cells, using a Na metal disk as a quasi-reference electrode. The voltammograms were scanned between 0.1 and 10 mVs^{-1}. These electrochemical experiments were monitored in a VMP Biologic instrument. The Electrochemical Impedance Spectra (EIS) were recorded on Swagelok™ type three-electrode cells bearing a Na metal disk as a pseudo-reference. Impedance spectra were after subsequent discharges at C/10 rate. After subjecting the cell to the galvanostatic pulses, the cell was allowed to relax for at least 2 hours before recording the spectrum on a SP-150 Biologic system. For this purpose, the open circuit voltage was perturbed with an AC signal of 5 mV from 100 kHz to 0.001 mHz. A full sodium-ion cell was assembled with the graphitic CNF as a negative electrode and C@$Na_3V_2(PO_4)_3$ as a positive electrode. The latter electrode consisted of the active material 80%, carbon black 10% and PVDF 10%. The preparation was identical to that of CNF, though an aluminum disk was used as a substrate. The electrolyte was identical to the half cells. Capacity values of the full cell were referred to the active mass of the cathode material. In order to avoid the irreversibility of the first cycle, the CNF electrode was previously subjected to a first cycled versus Na metal in half-cell configuration at the same current density. After several tests with different electrode masses, the mass ratio of the active materials of the two electrodes was optimized to $m_+/m_-=1.2$.

Results and discussion

Electrochemistry in half-cells

The electrochemical behavior of Na/CNF half-cells is summarized in Figs. 1 and 2. Fig. 1A shows the voltage vs capacity curves recorded under galvanostatic conditions at C/7. The resulting average voltage is ca 0.8 V vs. Na.), the high voltage observed for the sodium-DGM intercalation can be an advantage in terms of battery safety as compared to the intercalation of lithium into graphite ca. 0.0-0.2 V.[32] During the first discharge process, the slope of the voltage curve is nearly constant in the region between 0.7 and 0.0 V. In contrast, the voltage profile exhibits changes in the slope during the first charge and successive cycles. The irreversibility observed in the first cycle suggests that around half of sodium is irreversibly trapped in CNF. After the initial irreversible capacity of the first few cycles, the efficiency is very good, and the cell can be largely cycled with very good capacity retention at several kinetics (Fig. 1 C and Fig. S1). According to the results shown in Fig. 1B and Fig. S1, at 1C both the charge and discharge capacity values are ca. 90-95 mA h g^{-1} at C rate, while at lower kinetics the capacity increases (up to ca. 150 mA h g^{-1} at C/33 rate). An excellent capacity retention (from 92 to 96 mA h g^{-1} in first and over 500 cycles) is obtained. It is observed that the discharge capacity is higher than the charge one. This result strongly suggests that there is some contribution to the discharge capacity of irreversible reactions such as electrolyte decomposition, particularly at low kinetics. In Fig. 1C, the reversible capacity is about 130 mA h g^{-1} at the slowest rate (0.025C) and ca. 80 mA h g^{-1} at the highest rate (10C). thus, the quasi-one-

dimensional morphology of CNF provides a short diffusion path for sodium insertion and hence allows fast charge and discharge. For the sake of comparison, we also tested the electrochemical behavior of a Na/CNF half-cell using a carbonate-based electrolyte, revealing a very poor performance (Fig. S1). Natural graphite, thermally expanded graphite and

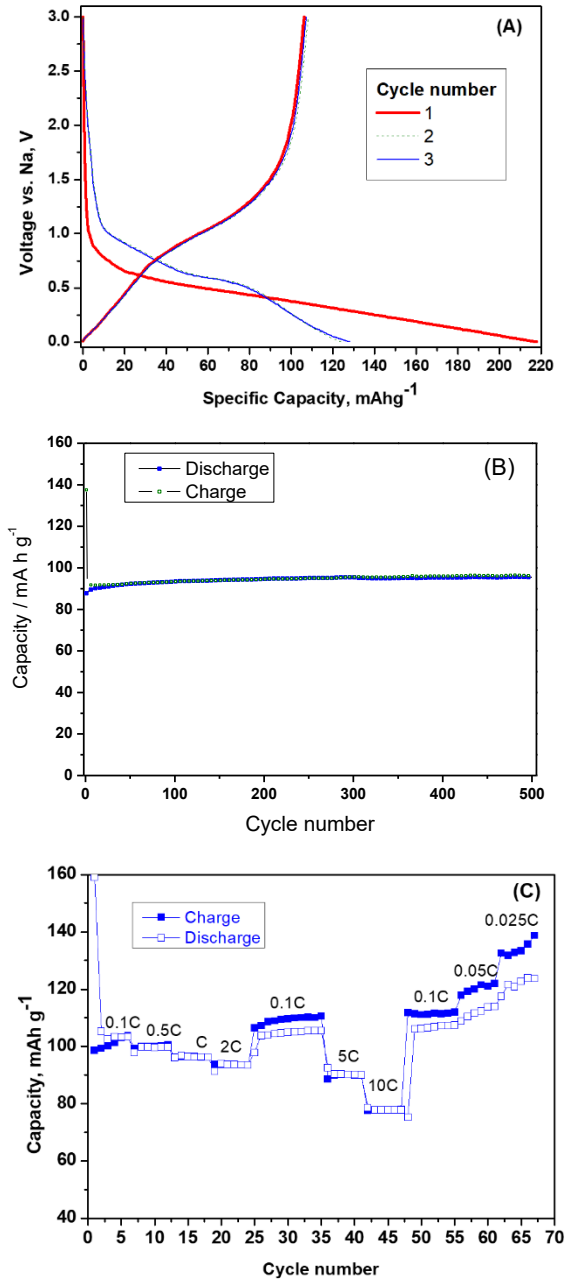

Figure 1. Electrochemical tests for galvanostatic cycling of Na/CNF half cells. (A) Voltage versus capacity curves at C/7 rate. (B) Gravimetric capacity versus cycle number at C rate. (C) Gravimetric capacity versus cycle number at several C/n rates. Voltage limits: 0.03-3.0 V.

graphitic petroleum coke were previously tested in Na cell using diglyme-based electrolytes.[14,33] Their reversible capacity is around 100-120 mA h g^{-1} at C rate. Recently, biogas-derived carbon nanofibers (BCNFs) have been investigated as anodes for sodium-ion batteries in a glyme-based electrolyte exhibiting stable capacity of 100 mA h g^{-1} at 37.2 mA g^{-1} (~C/4).[34] Our CNF exhibited lower capacity (90-95 mA h g^{-1}) at C rate, but at lower C rate exhibited capacity of 120 mA h g^{-1} (at C/7) and 150 mA h g^{-1} (at C/33). Ultimately, a full cell will be assembled by utilizing cathodes whose electrochemical performance is compatible with glyme-based electrolytes as for example $Na_{1.5}VPO_{4.8}F_{0.7}$, $Na_7V_4(P_2O_7)_4PO_4$ or $Na_3V_2(PO_4)_3$.[33,35] From industrial point of view is desirable to produce high-voltage NIBs that can compete with LIBs in terms of energy density. As a conclusion, although using diglyme is a great advance as compared to other solvents, the electrolyte solution should be further optimized.

In the CV plots, the first reduction sweep exhibits a broadened peak between ca. 0.6 and 0.0 V (Fig. 2A). This cathodic peak is irreversible and, consequently, it could be tentatively related to irreversible processes such as, electrolyte decomposition, irreversible trapping of sodium or microstructure change. Thus, both the galvanostatic and CV results suggest that an activation process takes place during the first discharge, as it is further discussed below. After the first cycle, the main cathodic peak is located at 0.53 V and the main anodic peak at 1.0 V. However, there are other small peaks, suggesting that there are several sites for accommodation of sodium in CNF.

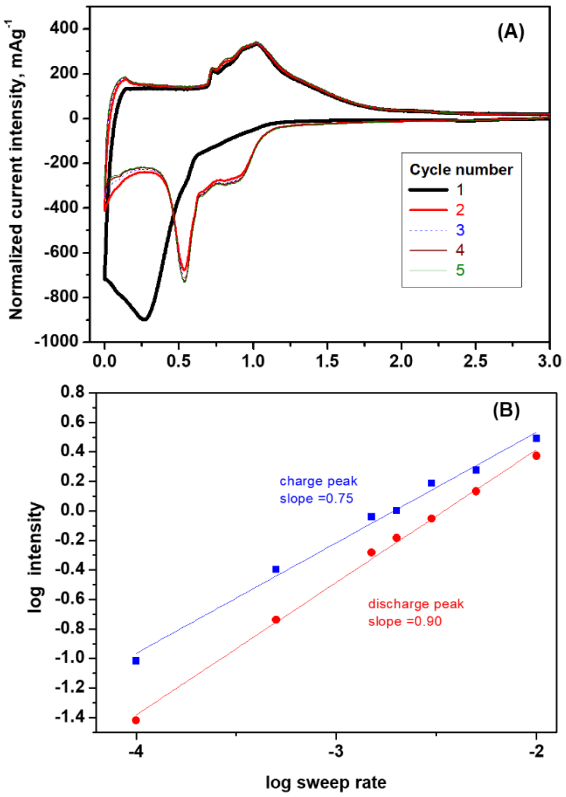

Figure 2. Electrochemical results for voltammetry experiments of CNF versus. Na in three-electrode cell. (A) Voltammograms obtained at 1 mV s^{-1}. (B) Determination of b-value for the main peak of the second scan during the charge (anodic peak) and discharge (cathodic peak).

Interesting information about the nature of the sodium electrochemical reaction can be inferred from the

determination of the elucidation of the relative contribution of faradic and capacitive processes in the electrode along the cell potential window. The relationship between the intensity of the main peak (I) and the applied sweep rate (v) is defined by the following equation:

$$I = a\, v^b \quad (1)$$

By applying logarithm to equation (1), we can find a linear relationship as follow:

$$\log I = \log a + b \log v \quad (2)$$

Thus, the parameter b can be calculated from the slope of the graphical plotting of logarithm of intensity (I) versus logarithm of sweep rate (v) (Fig. 2B).[36] This procedure was applied to the second discharge and charge. A b value equal to 1.0 corresponds to a surface-controlled capacitive process, while b= 0.5 involves a diffusion-controlled faradic process. In our calculations, we determined a value of b=0.90 and b=0.75 for the main peaks of the second discharge and charge, respectively. These results indicate that the mechanism is intermediate between capacitive and faradic, but the capacitive process is more relevant, unless in the second cycle. This result indicates that the reaction is not limited by the intercalation process, because the intercalation process is very easy due to DGM-coordination. The nanometric character and the morphology of the fibers also could contribute to the apparent surface-control. Similarly, Ramos et al also found two types of control for reaction between sodium and expanded graphite.[37]

Sodiated carbon nanofibers

The XRD pattern of raw CNF evidences the graphitic character of this material (Fig. 3a).[25] The peak at ca. 26.6°2θ is ascribable to the reflection (002) of graphite, and applying the Scherrer equation to its broadening, the resulting average crystallite size is Lc = 30 nm. The asymmetry of this peak can be due to microstrains and changes in the stacking of the graphene layers in the graphitic domains of CNF.[38] During the first discharge (referred as d1 in Fig. 3 b, d), the reflection (002) is progressively shifted to lower angles, due to sodium intercalation, and hence interlayer space expansion. The broadening and low-intensity of this peak reveal loss of crystallinity of the graphitic domains, most probably related to the irreversible capacity of the first cycle. During the second discharge (referred as d2 in Fig. 3 d, e) the shift of the reflection (002) to lower angles is even longer, suggesting the transformation of the structure. It will be further discussed at the light of the electron micrographs. At the end of the second discharge (Fig. 3e), the positions of the reflections at ca. ca. 15.3° and 23° 2θ agree well with the appearance of a phase stage-I. Stages of higher indexes, which emerge below 15°2θ, are not observed. Due to the lack of preferred orientation in the CNF, reflections (004), (005), (006), etc. are not observed, in contrast to other graphitic materials with layered-type morphology[33] and, consequently, a Patterson diagram could not be calculated. After the second charge (c2 in Fig. 3f) the (002) reflection is shifted back to ca. 26°2θ, in good agreement with the reversible extraction of sodium. The reflections of stage-I are again observed after 20 cycles (Fig. 3g). The staging mechanism observed in Fig. 2e and g needs an activation process, because it is not observed during the first discharge, in good agreement with the electrochemical results discussed above. This activation process was not observed in other graphite samples,[33] and it is related to the special microstructure of the CNF.

The EPR spectrum of pristine CNF (Fig. 4) consists of the superposition of two signals with different linewidth: an intense narrow isotropic line centered at g=2.003, and a broad anisotropic line at about g=2.01. The narrower line, with symmetric Lorentzian shape, is ascribed to localized carbon-related paramagnetic centers. Their origin is commonly ascribed to dangling bonds with unpaired electrons located at in the edges of graphene sheets.[34] In turn, the broadest line is ascribed to conduction electrons in graphitic nanodomains. After the first discharge, the relative intensity of the narrow line decreases, and the intensity of the broadened line increases. After the second discharge, the broad line exhibits even higher intensity. The sodium ions are trapped by dangling bonds, resulting in covalent C-Na bonds, involving the disappearance of this signal in the sodium intercalated phase carbons.[35]

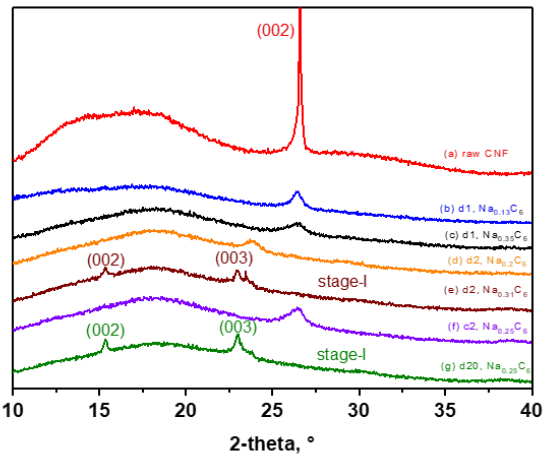

Figure 3. A detailed view of the XRD patterns for (a) raw CNF and electrodes retrieved from the electrochemical cell at selected states of (b, c) the first discharge, (d, e) second discharge, second charge and (f) twentieth discharge.

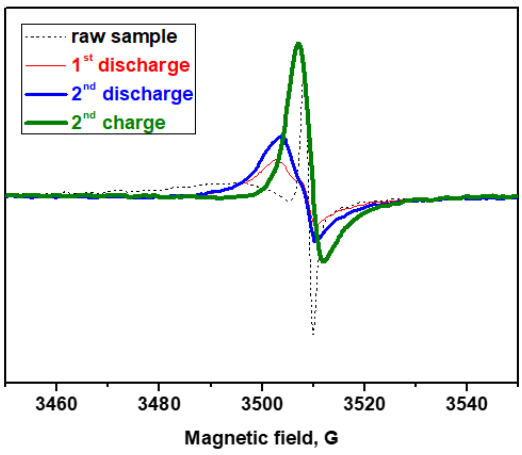

Figure 4. EPR of raw CNF, after first discharge and after second discharge.

In addition, the line shape of the sodiated CNF is Dysonian. These results mean that the reduction process and the intercalation of sodium yield to an increase of the unpaired delocalized electrons in the graphene sheets, similarly to lithium intercalation. When the electron concentration is high enough to produce the skin-depth effect, the high electronic conductivity in graphitic materials results in asymmetric Dysonian line shape. After the second discharge, there are more delocalized unpaired electrodes in the graphitic domains. After the second charge, an asymmetric EPR line with Dysonian shape is observed, which is typical of conduction electrons in graphitic domains.[41] The signal of paramagnetic centers is not observed.

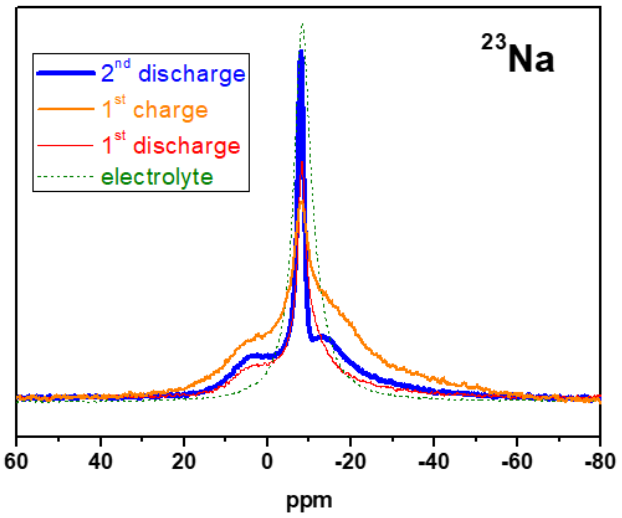

Figure 5. ^{23}Na MAS NMR spectra for CNT impregnated with the electrolyte solution, after the first discharge, first discharge-charge cycle, and after the second discharge.

NMR spectroscopy has been previously performed to study the intercalation of sodium into graphite.[16] Here we recorded ^{23}Na NMR spectra of sodium intercalated graphitized CNF (Fig. 5). The narrower and intense peak centred at -8 ppm observed in all the spectra is ascribed to electrolyte salt remaining onto the electrode even after washing. To verify this assumption, the spectrum of the CNF sample freshly impregnated with electrolyte solution was also recorded. The spectrum obtained after the first discharge also exhibits a low-intensity and broad peak at ca. +5 ppm. Previous reports on ^{23}Na studies of Na in disordered carbons have associated this peak to sodium weakly adsorbed in the spaces between misaligned graphene sheets and/or in closed nanopores.[16,42,43] After cell charging, the spectrum shows a third broad peak at ca. -14 ppm, which is usually assigned to Na ions either strongly adsorbed on the graphite surface or irreversibly trapped inside the graphite. Likely, this peak is also present in the discharged sample but masked by the presence or reversibly intercalated sodium at +5 ppm. Only after extracting the latter ions on charging, the presence of Na irreversibly trapped is evidenced in the charge electrode. After the second discharge-charge cycle, the spectrum becomes broadened due to traces of electrolyte and irreversibly trapped sodium. The trapped sodium could be on the surface of the carbon or intercalated in the graphitic domains. This line broadening is due to the increase of the magnetic susceptibility or to non-symmetric environments around the Na ions could contribute to this effect.[16] Thus, the coordination of two molecules of DGM by each Na atom.[39]

The intercalation mechanism found in this manuscript is very similar to that found in thermally expanded graphite and petroleum coke.[19,33] Irrespective of achieving slightly higher capacity for thermally expanded graphite and graphitic petroleum coke (100 – 120 mA h g^{-1}) than for CNF (90 – 95 mA h g^{-1}) similarities in the ex-situ XRD patterns are observed (Fig. 3 of the present manuscript and Fig. 8-9 in Ref# 19 and Fig. 5 in Ref.#33). Therefore, after a first discharge, a new set of (00l) reflection appeared, which are indexed as belonging to the Stage-1 of the $Na_x(DGM)_2C_{20}$ compound [Ref.#14 and #17]. Thus, it evidences the co-intercalation of both sodium ions and diglyme solvent into CNF. Electrochemical, XRD, TEM, NMR and EPR characterization suggest that an activation process occurs during the first discharge: The insertion of sodium induces strains and swelling that eventually breaking the fibers providing new paths for the sodium access to the interlayer space. This facilitates further access of sodium in further cycles.

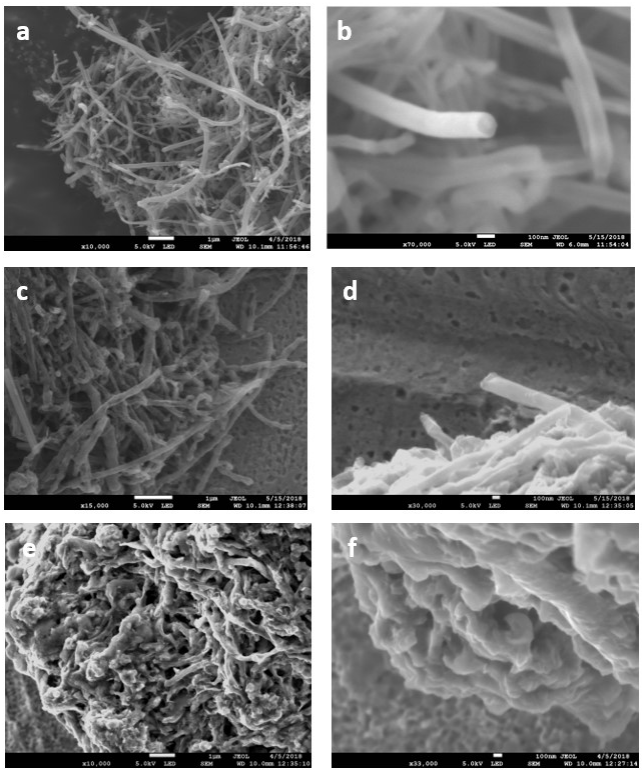

Figure 6. FESEM images of CNF (a, b) raw sample, (c, d) after two cycles and (e, f) after fifty cycles.

In order to study the effect of the electrochemical cycling in the morphology of the CNF, FESEM and TEM images are shown in

Figs.6 and 7. The mean diameter of the fibers is about 150 nm (Fig. 6a, b), and the central part of the fibers exhibits a cavity of ca. 50 nm diameter that runs parallel to the tube axis. Some of the tips were observed to be open. Due to the electrochemical cycling, the axial morphology of the CNF is progressively altered

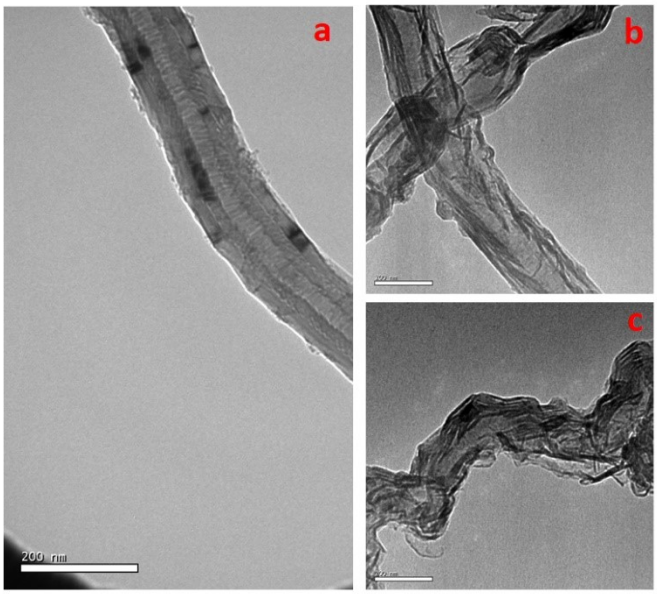

Figure 7. TEM images of (a) raw CNF and (b, c) after two discharge-charge cycles.

(Fig. 6c-f and 7). After the second cycle, the TEM images (Fig. 7) unveils that the walls of the CNF are wrinkled. After 50 cycles (Fig. 6e-f), the axial morphology of the CNF is hardly observed, and the wrinkled nanofibers yield to sponge-like agglomerates. Due to the insertion of sodium and DGM, microstrains and swelling are induced, eventually breaking the fibers. Similarly, it was found previously that the mechanism of lithium insertion into graphitized CNF involves, besides staging phenomena, irreversible collapse of the graphitic domains.[25] Compared to lithium, intercalation of sodium-DGM is affecting even more the structure of the CNF. Notwithstanding, the observed deterioration of the nanotube morphology is not harmful for the electrochemical cycling, because of the capacity retention evidenced in Fig.1. Most probably, the initial insertion of sodium-diglyme breaks the walls of the nanofibers, facilitating sodium accessibility of the active redox centers. Thus, stage-I is observed in the XRD patterns after the second discharge and later, but not in the first discharge.

Impedance spectra provide helpful information about kinetic response of electrode materials. Particularly, values of the internal resistances existing at the electrode-electrolyte interphase can be calculated when the Nyquist plots are fitted to an equivalent circuit (Fig. 8). Their profiles feature a semicircle at high-frequency region, a distorted semicircle at intermediate frequencies, and a sloping line at low-frequency range. The semicircle at high frequencies is ascribed to the migration of ions through the passivating film deposited of the CNF surface during the irreversible reactions occurring the first discharge. The region at medium frequencies is associated to the charge-transfer reaction between electrons and Na^+ at the active material surface. The sloping line at low frequencies is ascribed to sodium diffusion into the structure of the host material. In this way, all those diffusivity processes affecting the migration of Na^+ from the electrolyte solution towards the bulk of the electrolyte are regarded. The main difference between the first and the second discharge is the decrease of impedance for the charge transfer reaction after the second discharge. In our results R_{SEI} is 5 and 4.5 Ohm in first and second discharge. However, R_{CT} changes from 8 to 5 Ohm, respectively (Fig.8). This fact involves that the kinetic of the sodium intercalation is improved. In fact, the capacity increases slightly from 92 to 96 mA h g-1 over 500 cycles (Fig1 b). Such activation results from strains generation and swelling during cycling, that eventually break the fibers providing new paths for the sodium access to the interlayer space. This facilitates further access of sodium in further cycles. Kim et al.[35] reported that ether-based electrolytes could suppress electrolyte decomposition, resulting in formation of a negligible SEI film (R_{SEI} ~ 5 Ohm) on the graphite surface, enabling Na^+ -solvent transport to the graphite lattice. On the contrary, carbonate-based electrolytes form relatively thick insulating SEI layers (R_{SEI} ~ 250 ohm) on the graphite surface, which block Na^+ -solvent transport (Figure 4 f,g in Ref.#35). This fact involves that the kinetic of the sodium intercalation is improved, as could be expected from an activation process, likely provided by DGM cointercalation.

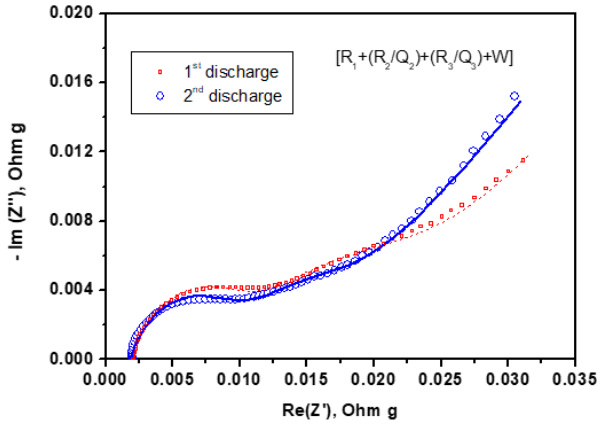

Figure 8. Nyquist plots (symbols) and the corresponding fitting (lines) with the equivalent circuit shown inside.

Full sodium-ion battery

The validity of this graphitize carbon nanofiber as negative electrode in a full sodium-ion battery was galvanostatically tested (Fig. 9). The average discharge voltage of the battery is about 2.2 V and a discharge capacity of 96 mA h g^{-1} was recorded with a coulombic efficiency of 87%. From the latter values an energy density of 210 W h kg^{-1} can be inferred. These

finds confirm that graphitized nanocarbons, such as graphitic carbon nanofibers, can be used in sodium-ion batteries.

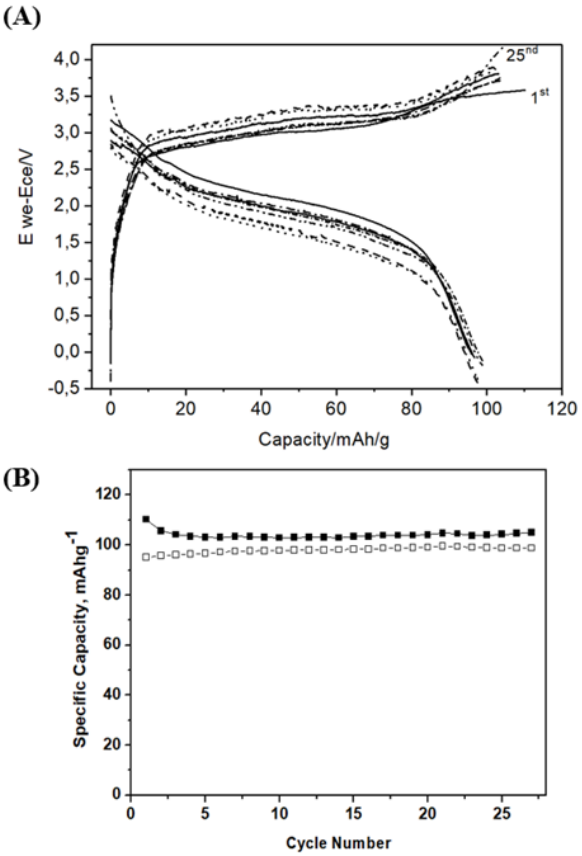

Figure 9. A) Full sodium-ion cell assembled with the graphitic CNF as a negative electrode and C@$Na_3V_2(PO_4)_3$ as a positive electrode using 1M $NaPF_6$ in diglyme. B) Its capacity retention.

Conclusions

For the first time, a graphitized carbon nanofiber has been electrochemically tested as a potential anode for sodium ion batteries. Electrochemical cycling in sodium half cells revealed that the use of a diglyme-based electrolyte allows the reversible insertion of sodium at an average potential of 0.8 V. Despite of the initial irreversibility, reversible capacity as high as 150 mA h g^{-1} was recorded with very good capacity retention at several kinetics. Electrochemical test suggest that an activation process occurs during the first discharge, which facilitates further access of sodium in further cycles. This assumption was confirmed by the analysis if the electron microscopy images revealing that the insertion of sodium induces strains and swelling that eventually breaking the fibers providing new paths for the sodium access to the interlayer space. It was evidenced by the decrease of cell impedance. The significance of surface effects on the sodium insertion was evidenced by the analysis of cyclic voltammograms, which unveiled the remarkable contribution of capacitive effects to the overall capacity.

X-ray diffraction of cycled electrodes showed that activation process is reflected by the appearance of a phase stage-I during the second discharge, which is preserved in further cycles. In addition, EPR and ^{23}Na NMR spectra evidenced the significant role of localized carbon-related paramagnetic centers to trap sodium near the surface, though the contribution of signals attributable to sodium reversibly inserted in discharged electrodes is notorious enough to justify the good electrochemical performance. For the first time, we have evidenced the reliability of a graphitized carbon nanofiber as negative electrode in a full sodium-ion battery. An average discharge voltage of 2.2 V and an energy density of 210 W h kg^{-1} allow us to conclude that the concept of this new sodium ion battery could be competitive.

Conflicts of interest

There are no conflicts to declare.

Acknowledgements

The authors are grateful to *Ministerio de Economía, Industria y Competitividad* (MINECO, MAT2017-84002-C2-1-R), ERDF funds and J*unta de Andalucía* for financial support (group FQM288). We also thank SCAI (UCO Central Service for Research Support).

Notes and references

1 P. K. Nayak, L. Yang, W. Brehm and P. Adelhelm, *Angew. Chem. Int. Ed.*, 2018, **57**, 102.
2 M. J. Aragón, P. Lavela, G. Ortiz, R. Alcántara and J. L. Tirado, *J. Alloys Compd*., 2017, **724**, 465.
3 M. J. Aragón, P. Lavela, G. F. Ortiz, R. Alcántara and J. L. Tirado, *Chem. Eur. J.*, 2017, **23**, 7345.
4 L. Yu, L. P. Wang, H. Liao, J. Wang, Z. Feng, O. Lev, J. S. C. Loo, M. T. Sougrati and Z. J. Xu, *Small* 2018, **14**, 1703338.
5 K. Kubota, M. Dahbi, T. Hosaka, S. Kumakura and S. Komaba, *Chem. Rec.*, 2018, **18**, 1.
6 J. Wang, T. Xu, X. Huang, H. Li and T. Ma, *RSC Adv.*, 2016, **6**, 87778.
7 R. Alcántara, F. J. Fernández Madrigal, P. Lavela, J. L. Tirado, J. M. Jiménez-Mateos, C. Gómez de Salazar, R. Stoyanova and E. Zhecheva, *Carbon*, 2000, **38**, 1031.
8 N. Sun, H. Liu and B. Xu, *J. Mater. Chem. A*, 2015, **3**, 20560.
9 C. Bommier, W. Luo, W.-Y. Gao, A. Greaney, S. Ma and X. Ji, *Carbon*, 2014, **76**, 165.
10 R. Alcántara, J. M. Jiménez-Mateos, P. Lavela and J. L. Tirado, *Electrochem. Commum*., 2001, **3**, 639.
11 C. Vidal-Abarca, P. Lavela, J. L. Tirado, A. V. Chadwick, M. Alfredsson and E. Kelder, J. Power Sources 2012, 197, 314.
12 Y. Liu, Boris V. Merinov, and W. A. Goddard III, *Proc. Natl. Acad. Sci. USA* 2016, **113**, 3735.
13 Hiroki Moriwake, A. Kuwabara, Craig A. J. Fisher and Yuichi Ikuharadue, *RSC Adv.,* 2017, **7**, 36550.
14 B. Jache and P. Adelhelm, *Angew. Chem. Int. Ed.*, 2014, **53**, 10169.
15 H. Kim, G. Yoon, K. Lim, K. Kang*, Chem. Commun.,* 2016, **52**, 12618—12621.

16 N. Leifer, M. F. Greenstein, A. Mor, D. Aurbach and G. Goobes, *J. Phys. Chem. C*, 2018, **122**, 21172.
17 Z. Zhu, F. Cheng, Z. Hu, Z. Niu and J. Chen, *J. Power Sources*, 2015, **293**, 626.
18 I. Hasa, X. Dou, D. Buchholz, Y. Shao-Horn, J. Hassoun, S. Passerini and B. Scrosati, *J. Power Sources*, 2016, **310**, 26.
19 M. Cabello, X. Bai, T. Chyrka, G. F. Ortiz, P. Lavela, R. Alcántara and J. L. Tirado, *J. Electrochem. Soc*., 2017, **164**, A3804.
20 C. Bommier, D. Mitlin, and X. Ji, *Prog. Mater. Sci.*, 2018, **97**, 170.
21 J. Zhang, D. W. Wang, W. Lv, S. Zhang, Q. Liang, D. Zheng, F. Kang, and Q. H. Yang, *Energy Environ. Sci*., 2017, **10**, 370.
22 J. Zhang, D. W. Wang, W. Lv, L. Qin, S. Niu, S. Zhang, T. Cao, F. Kang, and Q. H. Yang, *Adv. Energy Mater*. 2018, **8**, 1801361.
23 K. Li, J. Zhang, D. Lin, D. W. Wang, B. Li, W. Lv, S. Sun, Y. B. He, F. Kang, Q. H. Yang, L. Zhou, and T. Y. Zhang, *Nat. Commun.,* 2019, **10**, 725.
24 M.-S. Balogun, Y. Luo, W. Qiu, P. Liu, Y. Tong, *Carbon*, 2016, **98**, 162.
25 Y. Cao, L. Xiao, M.L. Sushko, W. Wang, B. Schwenzer, J. Xiao, Z. Nie, L. V. Saraf, Z. Yang and J. Liu, *Nano Lett*., 2012, **12**, 3783.
26 H. Song, N. Li, H. Cui and C. Wang, *Nano Energy*, 2014, **4**, 81.
27 M. Hao, N. Xiao, Y. Wang, H. Li, Y. Zhou, C. Liu and J. Qiu, *Fuel Processing Technology*, 2018, **177**, 328.
28 Z. Chen, T. Wang, M. Zhang and G. Cao, *Small*, 2017, **13**, 1604045.
29 X. Sun, C. Wang, Y. Gong, L. Gu, Q. Chen and Y. Yu, *Small,* 2018, ***14***, 1802218.
30 V. Subramanian, Hongwei Zhu, and Bingqing Wei, *J. Phys. Chem. B,* 2006, **110**, 7178.
31 R. Klee, M. J. Aragón, R. Alcántara, J. L. Tirado and P. Lavela, *Eur. J. Inorg. Chem*., 2016, **2016**, 3212.
32 I. Cameán, P. Lavela, J. L. Tirado and A. B. García, *Fuel*, 2010, **89**, 986.
33 M. Cabello, T. Chyrka, R. Klee, M. J. Aragón, X. Bai, P. Lavela, G. M. Vasylchenko, R. Alcántara, J. L. Tirado and G.F. Ortiz, J. Power Sources, 2017, 347, 127.
34 C. Menachem, Y. Wang, J. Flowers, E. Peled and S. G. Greenbaum, *J. Power Sources*, 1998, **76**, 180.
35 R. Alcántara, G. F. Ortiz, P. Lavela, J. L. Tirado, R. Stoyanova and E. Zhecheva, *Chem. Mater*., 2006, **18**, 2293.
36 I. Camean, J. Rodríguez García, and A. B. García. *J. Electrochem. Soc.,* 2019, **166**, A403.
37 H. Kim, J. Hong, Y. Park, J. Kim, I. Hwang, K. Kang, *Adv. Funct. Mater.* 2015, **25**, 534.
38 T. Brezesinski, J. Wang, J. Polleux, B. Dunn and S. H. Tolbert*, J. Am. Chem. Soc*., 2009, **131**, 1802.
39 A. Ramos, I. Cameán, N. Cuesta, C. Antuña and A. B. García, *Electrochim. Acta*, 2016, **187**, 496.
40 R. Alcántara, P. Lavela, G. F. Ortiz, J. L. Tirado, E. Zhecheva and R. Stoyanova, *J. Electrochem. Soc.,* 2007, **154**, A964.
41 E. Zhecheva, R. Stoyanova, J. M. Jiménez-Mateos, R. Alcántara, P. Lavela and J. L. Tirado, Carbon, 2002, 40, 2301.
42 R. Alcantara, P. Lavela, G. F. Ortiz and J. L. Tirado, *Electrochem. Solid-State Lett*., 2005, **8**, A222.
43 K. Gotoh, T. Ishikawa, S. Shimadzu, N. Yabuuchi, S. Komaba, K. Takeda, A. Goto, K. Deguchi, S. Ohki, K. Hashi, T. Shimizu and H. Ishida, *J. Power Sources*, 2013, **225**, 137.
44 K. Gotoh, H. Maruyama, T. Miyatou, M. Mizuno, K. Urita and H. Ishida, *J. Phys. Chem. C*, 2016, **120**, 28152.

